NeuroImage: Clinical 36 (2022) 103218

Contents lists available at ScienceDirect

NeuroImage: Clinical

journal homepage: www.elsevier.com/locate/ynicl

Effects of hyperbaric oxygen therapy on functional and structural connectivity in post-COVID-19 condition patients: A randomized, sham-controlled trial

Merav Catalogna [a], Efrat Sasson [a], Amir Hadanny [a,b], Yoav Parag [a], Shani Zilberman-Itskovich [a,b], Shai Efrati [a,b,c,*]

[a] Sagol Center for Hyperbaric Medicine and Research, Shamir (Assaf Harofeh) Medical Center, Zerifin, Israel
[b] Sackler School of Medicine, Tel- Aviv University, Tel-Aviv, Israel
[c] Sagol School of Neuroscience, Tel-Aviv University, Tel-Aviv, Israel

ARTICLE INFO

Keywords:
Post-COVID-19 condition
Brain connectivity
Resting state fMRI
DTI
Cognition

ABSTRACT

Introduction: Post-COVID-19 condition refers to a range of persisting physical, neurocognitive, and neuropsychological symptoms after SARS-CoV-2 infection. Abnormalities in brain connectivity were found in recovered patients compared to non-infected controls. This study aims to evaluate the effect of hyperbaric oxygen therapy (HBOT) on brain connectivity in post-COVID-19 patients.

Methods: In this randomized, sham-controlled, double-blind trial, 73 patients were randomized to receive 40 daily sessions of HBOT (n = 37) or sham treatment (n = 36). We examined pre- and post-treatment resting-state brain functional magnetic resonance imaging (fMRI) and diffusion tensor imaging (DTI) scans to evaluate functional and structural connectivity changes, which were correlated to cognitive and psychological distress measures.

Results: The ROI-to-ROI analysis revealed decreased internetwork connectivity in the HBOT group which was negatively correlated to improvements in attention and executive function scores ($p < 0.001$). Significant group-by-time interactions were demonstrated in the right hippocampal resting state function connectivity (rsFC) in the medial prefrontal cortex ($P_{FWE} = 0.002$). Seed-to-voxel analysis also revealed a negative correlation in the brief symptom inventory (BSI-18) score and in the rsFC between the amygdala seed, the angular gyrus, and the primary sensory motor area ($P_{FWE} = 0.012, 0.002$). Positive correlations were found between the BSI-18 score and the left insular cortex seed and FPN (angular gyrus) ($P_{FWE} < 0.0001$). Tractography based structural connectivity analysis showed a significant group-by-time interaction in the fractional anisotropy (FA) of left amygdala tracts ($F = 7.81$, $P = 0.007$). The efficacy measure had significant group-by-time interactions ($F = 5.98$, $p = 0.017$) in the amygdala circuit.

Conclusions: This study indicates that HBOT improves disruptions in white matter tracts and alters the functional connectivity organization of neural pathways attributed to cognitive and emotional recovery in post-COVID-19 patients. This study also highlights the potential of structural and functional connectivity analysis as a promising treatment response monitoring tool.

1. Introduction

The ongoing respiratory syndrome coronavirus 2 (SARS-CoV-2) pandemic has resulted in a highly prevalent new global long-term condition, defined by the World Health Organization as post-COVID-19 condition (Ceban et al., 2022; Herridge and Azoulay, 2022; Michelen et al., 2021). This condition is confirmed three months from the onset of COVID-19 with having symptoms that persist for more than two months and cannot be explained by an alternative diagnosis (WHO, 2019). Moreover, a recently published systematic review revealed that multiple physical, cognitive, and mental health symptoms persist for at least one year in a sizeable proportion of COVID-19 survivors (Han et al., 2022).

There is growing evidence that abnormalities seen in brain imaging are highly associated with the neurological sequelae of COVID-19. In the

* Corresponding author at: Sagol Center for Hyperbaric Medicine and Research, Shamir (Assaf Harofeh) Medical Center, Zerifin, Israel.
E-mail address: efratishai@outlook.com (S. Efrati).

https://doi.org/10.1016/j.nicl.2022.103218
Received 8 August 2022; Received in revised form 29 September 2022; Accepted 1 October 2022
Available online 3 October 2022

acute stage, neuroimaging studies show the presence of a wide range of cerebrovascular pathologies: micro and macro-bleeds, cerebral swelling, and hemorrhage in gray matter (GM) and white matter (WM) (Egbert et al., 2020; Katal et al., 2021). Recent review studies have revealed predominant involvement of the olfactory area, along with neighboring brain regions, including the prefrontal and limbic regions, in recovered COVID-19 patients, two to six months after infection. These studies have demonstrated structural and functional abnormalities including white matter hyperintensities (WMH), reduced gray matter volume, hypoperfusion, and microstructure changes (Benedetti et al., 2021; Duan et al., 2021; Huang et al., 2022; Najt et al., 2021; Qin et al., 2021). A recent large-scale neuroimaging study using the UK biobank cohort identified longitudinal effects in structural and functional brain scans before and after mild infections with COVID-19, with an average 141 days between the infection and second imaging scan. The study demonstrated significant loss of gray matter in areas with high connectivity to the olfactory system: the parahippocampal gyrus, the lateral orbitofrontal cortex, and the insula, notably in the left hemisphere. Mean diffusivity differences in longitudinal effects between recovered patients and controls were seen mainly in the orbitofrontal cortex, anterior cingulate cortex, as well as in the left insula and amygdala (Douaud et al., 2021; Douaud et al., 2022). Dysregulations in resting state functional connectivity (rsFC) within and between major neural networks have been identified among COVID-19 survivors two weeks to six months after infection. These alternations were associated with cognitive deficits, fatigue, depression, psychological distress, and post-traumatic stress disorder (PTSD) symptoms (Benedetti et al., 2021; Esposito et al., 2022; Fu et al., 2021; Hafiz et al., 2022; Silva et al., 2021; Tu et al., 2021; Yildirim et al., 2022).

We have recently shown in a prospective, randomized sham-controlled trial that hyperbaric oxygen therapy (HBOT) improves dysexecutive functions, psychiatric symptoms and fatigue in post-COVID-19 condition patients (Zilberman-Itskovich et al., 2022). Clinical improvements were correlated with increased cerebral blood flow (CBF), increased gray-matter mean diffusivity (MD), and increased white-matter fractional anisotropy (FA) in frontal, parietal and limbic regions associated with cognitive and psychiatric roles. These findings are supported by pre-clinical and clinical studies demonstrating HBOT's neuroplasticity effects through multiple mechanisms including anti-inflammatory, mitochondrial function restoration, increased perfusion via angiogenesis and induction, proliferation and migration of stem cells (Brkic et al., 2012; Efrati and Ben-Jacob, 2014; Gottfried et al., 2021; Hadanny and Efrati, 2020; Rockswold et al., 2010).

The aim of the current study was to further evaluate HBOT's effect on rsFC in patients suffering from post-COVID-19 condition, and its correlation to cognitive and psychiatric symptoms, in a randomized, sham-controlled, double blind clinical trial.

2. Methods

2.1. Patients

Patients were at least 18 years old with reported post-COVID-19 cognitive symptoms that affected their quality of life and persisted for more than three months following an RT-PCR test confirming a symptomatic SARS-CoV-2 infection. Patients were excluded if they had a history of pathological cognitive decline, traumatic brain injury or any other known non-COVID-19 brain pathology. Participants were recruited through public announcements, and from post-COVID-19 clinics.

2.2. Trial design

A prospective randomized, double-blind, sham-controlled trial was conducted at the Shamir Medical Center (SMC), Israel. After signing an informed consent, patients were randomized to either HBOT or control groups at a 1:1 ratio according to a computerized randomization table, supervised by a blinded researcher. Evaluation procedures were done at baseline and 1–3 weeks after the last HBOT/control session. All evaluators were blinded to the patients' group allocation.

This study is part of a comprehensive post-COVID-19 condition study. Detailed overview of the methodology and results of the clinical outcomes are provided in the study protocol and in (Zilberman-Itskovich et al., 2022). The study was approved by SMC's Institutional Review Board (IRB) (No. 332–20-ASF) and all participants signed an informed consent prior to their inclusion. All research was performed according to the relevant guidelines and regulations.

2.3. Intervention

Both HBOT and sham protocols were administrated in a multi-place Starmed-2700 chamber (HAUX, Germany). The protocol comprised of 40 daily sessions, five sessions per week within a two-month period. The HBOT protocol included breathing 100 % oxygen by mask at 2ATA for 90 min with five-minute air-breaks every 20 min. Compression/decompression rates were 1.0 m/minute. The sham protocol included breathing 21 % oxygen by mask at 1.03 ATA for 90 min. To mask the controls, the chamber pressure was raised up to 1.2 ATA during the first five minutes of the session along with circulating air noise followed by decompression (0.4 m/minute) to 1.03 ATA during the next five minutes.

2.4. Outcome measures

The primary outcome of the study was the cognitive assessment as evaluated by the NeuroTrax computerized cognitive testing battery (NeuroTrax Corporation, Bellaire, TX). This assessment evaluates various cognitive domains including memory, executive function, attention, information processing speed, and motor skills. Cognitive scores were normalized for age, gender and educational levels (Doniger, 2007, 2012).

The brief symptom inventory (BSI-18) was used to evaluate psychological distress, based on three subscales: depression, anxiety, and somatization.

2.4.1. Brain imaging

Brain imaging MRI scans were performed on a MAGNETOM VIDA 3 T scanner, configured with 64-channel receiver head coils (Siemens Healthcare, Erlangen, Germany). The MRI protocol included 3D T2-weighted, 3D fluid attenuated inversion recovery (FLAIR), susceptibility weighted imaging (SWI), pre and post contrast high-resolution T1-weighted (MPRAGE), and diffusion tensor imaging (DTI) for structural WM connectivity determination.

Structural T1-weighted MRI scans were acquired for co-registration purposes using a T1-weighted 3D magnetization-prepared rapid gradient-echo (MPRAGE) sequence in sagittal plane with 1 mm isotropic resolution. Sequence parameters: TR: 2,000 ms, TE: 1.9 ms, flip angle: 9°, TI: 920 ms, FOV: 256 × 256, and 256 contiguous slices.

A total of 300 volumes (7:40 min) resting state fMRI scans were acquired using gradient-echo-planar imaging BOLD sequence. Scan parameters: TR: 1,500 ms, TE: 30 ms, flip angle: 90°, voxel size: 2.2x2.2x3.0 mm, distance factor: 25 %, FOV: 210, number of slices: 36, axial slices parallel to the AP-PC plane. During scanning, each participant was asked to remain still and relaxed, with eyes open, and without thinking of anything deliberate. Foam pads and earplugs were employed to reduce head motion and scanning noise.

Whole brain diffusion weighted images were acquired with the following parameters: sixty axial slices, slice thickness = 2 mm, voxel size = 2x2 mm, TR = 3400 ms, TE = 63 ms, and matrix = 248x128 mm, SMS factor = 3. Diffusion gradients were applied along 64 noncollinear directions (b = 1000 s/mm2) and seven volumes without diffusion weighting, including five volumes in read directions and two volumes in

Table 1
Baseline characteristics.

	HBOT	Control	P-VALUE
N	28	28	
Age (Y)	48.2 ± 10.6	48.2 ± 9.5	1.000
Males	15 (53.6)	7 (25.0)	0.054
Female	13 (46.4)	21 (75.0)	0.054
BMI (Kg/m^2)	27.0 ± 5.5	26.6 ± 5.1	0.760
Years of education	14.7 ± 2.5	14.9 ± 4.0	0.843
Marital status			
Single	3 (10.7)	7 (25.0)	0.295
Married	21 (75.0)	15 (53.6)	0.162
Divorced	2 (7.1)	5 (17.9)	0.422
Widowed	2 (7.1)	1 (3.6)	1.000
N of children	2.5 ± 1.3	2.1 ± 1.4	0.377
Employment status	3 (10.7)	3 (10.7)	1.000
Time from infection (days)	157.5 ± 74.5	171.5 ± 71.1	0.482
MoCA - cognitive assessment	25.9 ± 2.7	24.9 ± 3.4	0.222
Hospitalized*	4 (14.3)	4 (14.3)	1.000
High risk conditions			
BMI† > 30	9 (32.1)	8 (28.6)	1.000
Age > 60 Y	3 (10.7)	4 (14.3)	1.000
Cancer	0 (0.0)	0 (0.0)	1.000
Diabetes mellitus	0 (0.0)	1 (3.6)	1.000
Hypertension	4 (14.3)	2 (7.1)	0.669
Heart disease	1 (3.6)	1 (3.6)	1.000
Immune deficiency	0 (0.0)	0 (0.0)	1.000
Asthma	1 (3.6)	0 (0.0)	1.000
Other chronic lung diseases	0 (0.0)	0 (0.0)	1.000
Chronic liver disease	0 (0.0)	3 (10.7)	0.236
Chronic kidney disease	0 (0.0)	0 (0.0)	1.000
Hematologic disease\disorder	0 (0.0)	0 (0.0)	1.000
Chronic neurological impairment \disease	1 (3.6)	1 (3.6)	1.000
Smoking			
Current	0 (0.0)	0 (0.0)	1.000
Previous	8 (28.6)	4 (14.3)	0.329

Data presented as n (%); continuous data, mean ± SD; † The body-mass index is the weight in kilograms divided by the square of the height in meters.
* during COVID19 infection; MoCA, Montreal cognitive assessment.

phase direction to compensate for *EPI* distortions.

White matter hyperintensities (WMH) were assessed, by an experienced neuroradiologist, on axial 3D FLAIR images and rated according to the age-related white matter change and Fazekas scales (standard 4-point scales) (Fazekas et al., 1987).

2.4.2. BOLD data preprocessing

Functional connectivity analysis was carried out using the CONN-fMRI toolbox v17 as implemented using statistical parametric mapping software SPM12 (https://www.fil.ion.ucl.ac.uk/spm). Functional volumes pre-processing pipeline included slice-timing correction, realignment, co-registration, normalization to MNI space (152-brain template) with a resolution voxel size of 2 × 2 × 2 mm, and spatial smoothing (8 mm FWHM Gaussian kernel) steps (Whitfield-Gabrieli and Nieto-Castanon, 2012). The preprocessing steps derived (1) the realignment covariate, containing the six rigid-body parameters characterizing the estimated subject motion, (2) the scrubbing covariate containing potential outlier scans performed with CONNs artifact detection tool (ART), and (3) the quality assurance (QA) covariate based on global signal change (>3 standard deviations from the mean image intensity) and framewise displacement (FD) scan-to-scan head-motion. Age and sex were also used as group (second level) covariates. A component-based noise correction procedure (CompCor) approach (Behzadi et al., 2007) was used to identify additional confounding temporal factors controlling for physiological noise, BOLD signal present in WM, and head motion effects. Finally, residual BOLD time series were then bandpass filtered at a frequency range of 0.01–0.1 Hz (Whitfield-Gabrieli and Nieto-Castanon, 2012). Individual connectivity maps were generated using the seed-to-voxel approach. We examined rsFC using a priori seeds derived from the FSL Harvard-Oxford atlas (Desikan et al., 2006), focusing on COVID-19 related commonly reported large-scale brain networks, which included: default mode (DMN), salience (SN), dorsal attention (DAN), fronto-parietal (FPN) (also known as central executive network, CEN), and sensorimotor (SMN). We also examined the rsFC of the hippocampus, amygdala and insula as seed ROIs, following the hypothesis of the involvement of these regions in post-covid symptoms (networks and the coordinates of the associated seed regions are presented in Supplementary Table 1). Bivariate correlation analysis was used to determine the linear association of the BOLD time series between the seed and significant voxel clusters. Fisher's Z transformation was applied to the correlation coefficients to satisfy normality assumptions. Then, functional connectivity maps were thresholded at $P < 0.05$ false discovery rate (FDR) corrected for multiple comparisons (Whitfield-Gabrieli and Nieto-Castanon, 2012). Finally, participants with head motions of > 2 mm in any direction between volumes, rotations of > 2° in any axis during scanning, or mean FD of > 0.5 in either the pre- or post-treatment maps were excluded from the dataset.

2.4.3. Adjusted ROI-to-ROI network analysis

We defined the adjusted ROI-to-ROI network analysis. We used the seeds described above (Supplementary Table S1) to conduct adjusted ROI-to-ROI network analysis to test connectivity within and between DMN, SNN, DAN, FPN and SMN networks. To overcome anatomical variations between patients, patient specific adjusted ROIs were derived as follows: in each map, a cluster was identified in within spheres of 6 mm radii centered on the coordinates of interest from each network. Then, the voxel with the maximal value within the sphere was identified as the adjusted ROI. For each corrected location, the mean Z-score value was calculated within a 3 mm radius. Inter-network and intra-network connectivity values were calculated producing a symmetrical 22 × 22 connectivity matrix. Analysis was performed using inhouse software written in MATLAB R2021b (MathWorks, Natick, MA).

2.4.4. DTI data analysis

Preprocessing of DWI images and DTI analysis was performed with ExploreDTI software (https://www.ExploreDTI.com) (Leemans et al., 2009) including regularization (denoising) motion and distortion correction.

A whole-brain structural connectivity matrix was computed using a network analysis tool implemented in the ExploreDTI software. We used the automated anatomical labeling (AAL) atlas as a template with 90 distinct regions of interest (ROIs) which were registered to each subject's dataset (Tzourio-Mazoyer et al., 2002). Tractography was performed between every inversely transformed AAL-ROI pair using the criteria of angle threshold > 45° and FA < 0.2. Then, 90x90 connectivity matrices (CMs) were derived according to the following variables: fractional anisotropy (FA), mean diffusion (MD), radial diffusion (RD), axial diffusivity (AD), linear anisotropy (Cl), planar anisotropy (Cp), and spherical anisotropy (Cs), average tract length, and density weight (Alexander et al., 2000; Hagmann et al., 2008). Whole brain density, and whole brain and regional efficacy were calculated using the brain connectivity toolbox (https://sites.google.com/site/bctnet/) (see Supplementary Materials for more details). Finally, we extracted tracts passing through either the left or the right ROIs: amygdala, hippocampus and insula, used as seed regions for MRI tractography, and calculated the total variable measure (Tv) of the ROI tracts (according to (Soravia et al., 2022):

$$T_V = \sum_{i=1}^{90} CM_{ROI,i}$$

where, CM is the connectivity matrix, ROI is the index in the AAL atlas, and V is the examined variable (FA, MD, RD, etc.).

2.5. Statistical analysis

2.5.1. Descriptive statistics

The demographics and clinical continuous data are expressed as means ± standard deviations (SD). Two-tailed independent t-tests were performed to compare variables between groups when a normality assumption held according to a Kolmogorov-Smirnov test. Categorical data were expressed in numbers and percentages, compared by chi-square/Fisher's exact tests. Data analysis was performed using MATLAB R2021b (MathWorks, Natick, MA) statistics and machine learning toolbox.

2.5.2. Imaging analysis statistic

At the group level, seed-to-voxel resting-state functional connectivity (rsFC) was analyzed using a mixed design repeated measure ANOVA model to test the main interaction effect between time and group. The analysis was implemented in SPM software (version 12, UCL, London, UK) with a non-parametric permutation-based (1000 permutation) analysis approach across the entire brain volume (Bullmore et al., 1999; Whitfield-Gabrieli and Nieto-Castanon, 2012). RsFC was considered significant at joint-probability thresholds of 0.001 at the voxel level, and $p < 0.05$ family-wise error (FWE) corrected for multiple comparisons across the whole brain at the cluster level, with a minimum cluster size of 50 voxels. The REX toolbox was used to extract cluster connectivity statistical values (Whitfield-Gabrieli and Nieto-Castanon, 2012). Wilcoxon rank-sum tests were used to test for differences in rsFC between the HBOT group and controls in the ROI-to-ROI analysis. The nonparametric effect size was calculated as Z divided by the square root of the number of observations (Fritz, 2011). P-values were corrected for multiple correlations based on a false discovery rate using the Benjamini-Hochberg FDR procedure ($P < 0.05$) (Benjamini and Hochberg, 1995). Spearman rank correlations were used to test for associations with cognitive and BSI-18 scores.

The structural connectivity group analysis was performed using a mixed design repeated measure ANOVA model to test the main interaction effect between time and group. Data analysis was performed using the MATLAB R2021b (MathWorks, Natick, MA) Statistics and Machine Learning Toolbox.

2.5.3. Sample size

The sample size was estimated on the basis of the primary outcome based on our recent study in healthy adults (Amir et al., 2020). A NeuroTrax global cognitive score improvement of 5.2 and 0.8 points, with a standard deviation of 6.7 points was found in the HBOT and control groups respectively. Assuming a power of 80 %, and 5 % two-sided level of significance, a total of 74 participants would be required, 37 participants in each arm. Considering a dropout rate of 15 % the total sample size required is 85.

3. Results

3.1. Patients

Ninety-one patients were eligible to participate in the study. Twelve patients did not complete baseline evaluations and the remaining seventy-nine were randomized to one of the two arms. Two patients from the control group withdrew their consent during treatment, and one patient was excluded due to poor compliance and did not complete the assessments. Two patients from the HBOT group were excluded, one due to intercurrent illness, and one due to a personal event that prevented completion of the protocol. An additional patient from the HBOT group withdrew his consent during treatment. Accordingly, 37 patients from the HBOT group and 36 patients from the control group completed the protocol and were included in the analysis. The patient flowchart and study timeline are presented in Supplementary Figure S1. No statistically significant differences between the two groups were observed in baseline characteristics. From the study sample, nine patients from the HBOT group and eight patients from the control group were excluded from further analysis due to excessive motion or head motion artifacts. Consequently, the final analysis included 28 patients from each group, and no significant difference in head motion was found between the groups (max translation, 1.02 ± 0.46 and 1.07 ± 0.41, $p = 0.549$, max rotation, 0.84 ± 0.44 and 1.00 ± 0.54, $p = 0.087$). The baseline characteristics of the patients are summarized in Table 1.

At baseline, 12 (54 %) patients had mild, and two patients had moderate WMH in the HBOT group, and 17 (47 %) patients had mild, and two patients had moderate WMH in the control group ($P = 0.642$) according to the Fazekas scale (Supplementary Table S2). There was no change in WMH analysis after HBOT or control sessions.

The results of the cognitive tests and BSI-18 questionnaires are detailed in our previous publication (Zilberman-Itskovich et al., 2022) and were used for correlation with the connectivity data. Briefly,

Table 2
ROI-to-ROI network analysis: changes in post-treatment functional connectivity in HBOT compared to controls.

	SEED	TARGET	P_{UNC}-value	P_{FDR}-value	Effect size
Decrease in rsFC					
Intra-network connectivity					
	SMN. Superior	SN.RPFC (R)	0.0001	0.024	−0.472
	SMN. Superior	SN.RPFC (L)	0.0004	0.049	−0.419
	SMN. Superior	SN.ACC	0.0007	0.057	−0.397
	SMN.Lateral (L)	SN.RPFC (L)	0.0018	0.061	−0.358
	SMN.Lateral (L)	SN.RPFC (R)	0.0031	0.060	−0.334
	SMN.Lateral (L)	FPN.LPFC (R)	0.0047	0.067	−0.314
	SN.AInsula (L)	FPN.LPFC (R)	0.0016	0.074	−0.364
	SN.ACC	DAN.FEF (R)	0.0018	0.068	−0.365
	SN.AInsula (L)	FPN.PPC (L)	0.0034	0.061	−0.329
	SN.RPFC (L)	DAN.FEF (L)	0.0043	0.071	−0.318
	DMN.LP (R)	FPN.LPFC (L)	0.0020	0.059	−0.354
	DMN.LP (R)	FPN.PPC (L)	0.0023	0.060	−0.347
Inter-network connectivity					
	FP.PPC (L)	FP.PPC (R)	0.0012	0.071	−0.375
Increase in FC					
Intra-network connectivity					
	S.RPFC/L	FP.LPFC/R	0.0030	0.063	0.336
Inter-network connectivity					
	SN.ACC	SN. Ainsula/L	0.0028	0.065	0.338
	SN.ACC	SN.RPFC/L	0.0045	0.069	0.316

Default mode (DMN), dorsal attention (DAN), fronto-parietal (FPN), salience network (SN), sensorimotor (SMN); BOLD $P_{FDR} < 0.05$, UNC, uncorrected, FDR. false discovery rate, R, right, L, left.

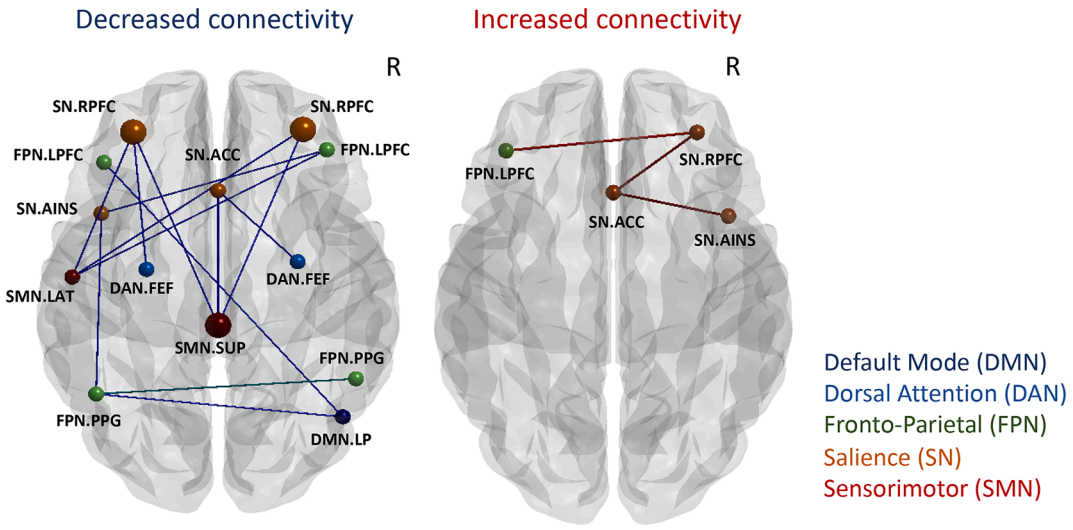

Fig. 1. ROI-to-ROI network analysis longitudinal group differences. Changes in post-treatment functional connectivity in the HBOT group compared to controls. Node color - network, node size – significance (see Table 2). Edge color: blue, inter-network connectivity; green, intra-network connectivity. Brain images were created using BrainNet Viewer software (http://www.nitrc.org/projects/bnv/). (For interpretation of the references to color in this figure legend, the reader is referred to the web version of this article.)

Table 3
Correlations between changes in rsFC and changes in cognitive scores.

connection		Cognitive index	r	P-value
SMN.Superior	SN.RPFC (L)	EF	−0.510	0.0001
DAN.FEF/R	SN.ACC	Attention	−0.453	0.0005
DAN.FEF (L)	SN.RPFC (L)	IPS	−0.441	0.0008
SMN.Superior	SN.RPFC (L)	Global	−0.374	0.0046
DMN.LP (R)	FPN.LPFC (L)	EF	−0.350	0.0081
SMN.Superior	SN.RPFC (L)	Motor skills	−0.343	0.0095
SN.AInsula (L)	FPN.LPFC (R)	EF	−0.306	0.0220
DMN.LP (R)	FPN.LPFC (L)	Attention	−0.304	0.0227
FPN.LPFC (L)	DMN.LP (R)	BSI-18	0.2781	0.0380
SN.AInsula (L)	FPN.LPFC (R)	Global	−0.273	0.0421
SN.RPFC (L)	SMN.Superior	BSI-18	0.263	0.0499

Default mode (DMN), dorsal attention (DAN), fronto-parietal (FPN), salience network (SN), sensorimotor (SMN), EF, executive function, IPS, information processing speed, BSI-18, BSI-18 questionnaire total score, r, Pearson's correlation coefficient, R, right, L, left.

following HBOT, there was a significant group-by-time interaction in global cognitive function, attention and executive function (d = 0.495, p = 0.038; d = 0.477, p = 0.04 and d = 0.463, p = 0.05 respectively). Improvement in psychological symptoms were also demonstrated after HBOT with significant group-by-time interaction and large effect size in the total BSI-18 score (d = 0.636, p = 0.008). Both somatization (d = 0.588, p = 0.014) and depression (d = 0.491, p = 0.04) scores showed significant group-by-time interactions.

3.2. ROI-to-ROI network analysis

Table 2 and Fig. 1 show group differences in rsFC. The ROI-to-ROI analysis revealed decreased SMN-SN connectivity between the superior primary motor area and bilateral rostral prefrontal cortex (RPFC) seeds (P_{FDR} = 0.024, 0.049, ES = -0.472, −0.419) in the HBOT group compared to controls. There was a trend-level reduction with a moderate effect size in the DMN-FPN connectivity between the right lateral parietal (LP) and left lateral prefrontal cortex (LPFC) and posterior parietal cortex (PPC) (p = 0.002, 0.0023, P_{FDR} = 0.059, 0.06, ES = -0.354 and −0.347), and in the sN-FPN connectivity between the left anterior-insula and the left posterior parietal cortex (PPC) (p = 0.0034, P_{FDR} = 0.061, ES = -0.365). Importantly, changes in NeuroTrax attention index negatively correlated to connectivity between DMN and FPN (r = -0.453, p = 0.0005), while changes in executive function index was negatively correlated to sN-SMN connectivity and sN-FPN connectivity (r = -0.510, −0.361, p = 0.0001, 0.007 respectively) (Table 3, Fig. 2). A trend-level hyperconnectivity was detected within the SN between ACC, anterior-insula and RPFC seeds, and sN-FPN between RPFC and LPFC seeds (Table 2, Fig. 1).

3.3. Seed-to-voxel based rsFC analysis of the hippocampus

Seed-to-voxel based functional connectivity analysis revealed a significantly increased rsFC in the HBOT group compared to the controls, as shown in Fig. 3. Significant group-by-time interactions were demonstrated in the right hippocampal and the left parahippocampal rsFC with the medial prefrontal cortex (DMN-MPFC, BA10) (T = -5.0, −4.19, P_{FWE} = 0.002, 0.024, respectively).

3.4. rsFC of the amygdala and the insula

Next, we investigated the relationship between cognitive and psychiatric scores, and the amygdala and insula maps using voxel-based analysis as shown in Table 4 and Fig. 4. Negative correlations were observed between the BSI-18 score and rsFN between the amygdala seed and FPN (angular gyrus) and SMN (primary sensory motor area) (P_{FWE} = 0.012, 0.002). Positive correlations were found between the BSI-18 score and the left insular cortex seed and FPN (angular gyrus) (P_{FWE} < 0.0001). Positive correlations with cognitive scores (IPS, EF) were found between the amygdala seed and the SN (supramarginal gyrus) and Broca area (a region suggested to part of the language network) (P_{FWE} < 0.05).

3.5. Structural connectivity of the amygdala

There were no significant differences between the groups in all the baseline structural connectivity measures (Table S3). There was a significant group-by-time interaction in the FA of left amygdala tracts post-HBOT compared to the control group (F = 7.81, P = 0.007) (Fig. 5). Additionally, Cl and efficacy measures had significant group-by-time interactions (F = 8.452, p = 0.005 and F = 5.98, p = 0.017 respectively) (Supplementary Table S3). No significant change was detected in the hippocampus and insula measures. There was no significant change in whole brain structural efficacy (F = 0.24, P = 0.628). There was a

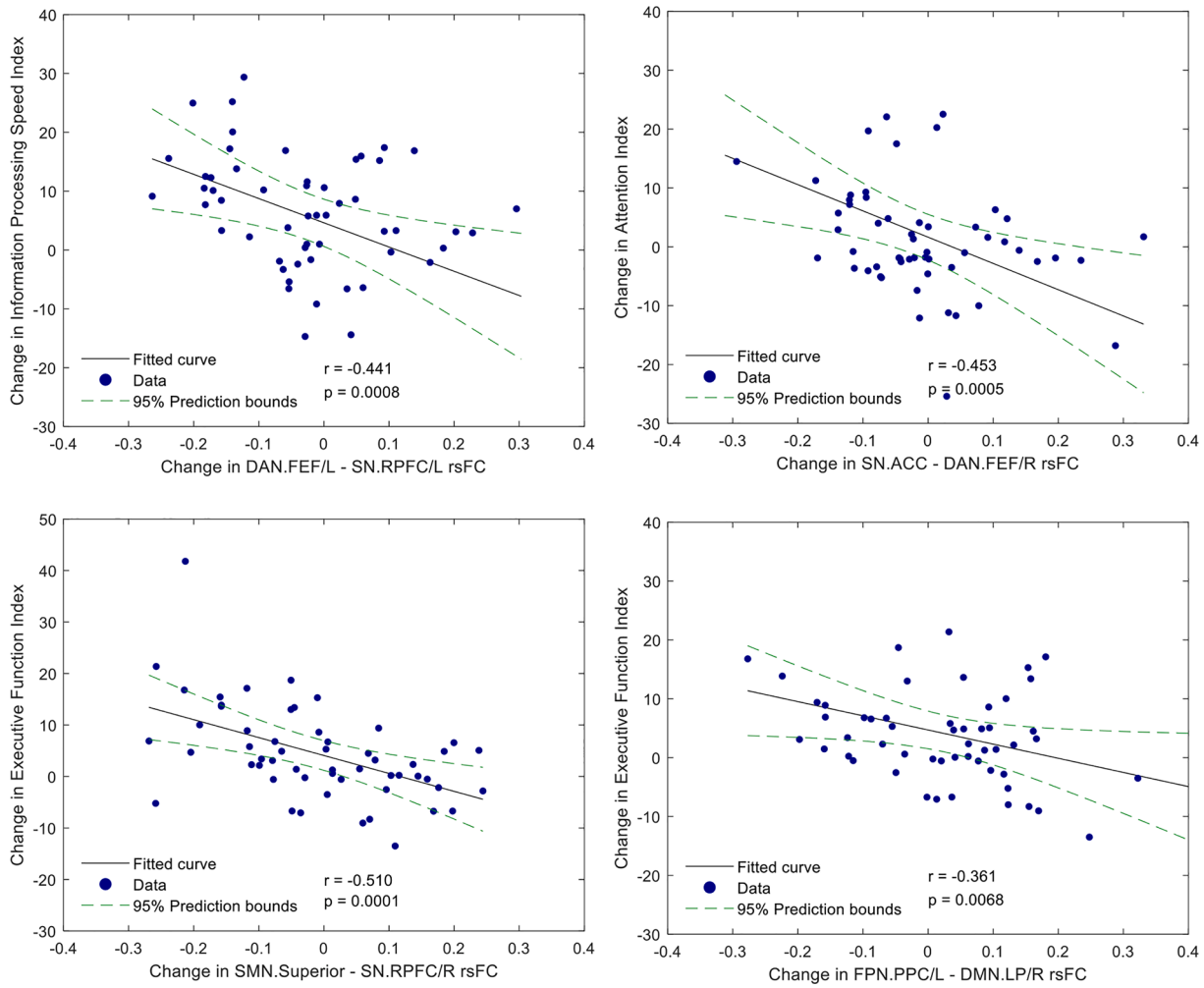

Fig. 2. ROI-to-ROI network analysis, correlation between longitudinal differences in rsFC and cognitive scores (n = 56). Scatterplot of the change in rsFC, and the change in executive function, attention, and information processing speed scores. The r is the Pearson's correlation coefficient. The 95 % prediction interval is presented as a green line. (For interpretation of the references to color in this figure legend, the reader is referred to the web version of this article.)

significant negative correlation between the left amygdala FA changes and changes in BSI-18 scores analyzed in the entire cohort (r = -0.350, p = 0.005), as shown in Fig. 5B.

4. Discussion

In this randomized sham-controlled trial, we identified longitudinal changes in cerebral network functional and structural connectivity during cognitive and emotional recovery in post-COVID-19 patients. We found that improvements in cognitive function induced by HBOT is correlated with reorganization and restoration of connectivity patterns between large-scale cognitive control networks. Moreover, enhancement in both functional connectivity and structural efficacy parameters of the amygdala circuit may reflect improvements in psychiatric symptoms related to post-COVID-19 condition.

Abnormalities in rsFC were found in individuals in the acute stage of severe to mild COVID-19 infection, but also in recovered patients compared to non-infected controls. Silva et al. (2021) detected internetwork hyperconnectivity in eleven large-scale networks in recovered individuals from mild infection. The most prominent effect was observed in the DAN (visuospatial) network connected to the left superior, parietal lobule, supramarginal gyrus, postcentral gyrus, and angular gyrus, and in the SN and DMN networks. In another study, increased connectivity was also detected in the DMN and DAN networks in patients in the acute stage. These changes were associated with cognitive impairment and increased inflammatory markers (Niroumand Sarvandani et al.). Increased time varying and topological organization between sensorimotor and visual networks were found in COVID-19 survivors six months after hospital discharge (Fu et al., 2021). In a study among post COVID-19 patients with a disorder of consciousness (DoC), significant reductions were observed in DMN intra-connectivity, but increased internetwork connectivity was found between DMN and SN networks (Fischer et al., 2022). Lastly, a study in recovered patients suffering from long lasting fatigue symptoms showed increased connectivity in the basal ganglia network within the occipital lobe and in the precuneus network in the precuneus and the superior parietal lobule (Hafiz et al., 2022). In our study, using HBOT, an opposite trend was demonstrated by reduced internetwork rsFC in the SMN and cognitive related networks (FPN, DMN, and SN), suggesting a potential reorganization and restoration of brain functional connectivity.

More specifically, the relationship between the FPN, DMN, and SN is known as a triple-network organization of cognitive function (Menon and D'Esposito, 2022; Menon, 2011). While the frontal cortex was found to play an important role in the coordination of cognitive control and executive function, the SN functions as an activating switch between the FPN and DMN when external or internal stimuli occurs respectively (Miller and Cohen, 2001). Previous studies have shown that hyperconnectivity is a common response to neurological disruptions associated with cognitive decline (Eyler et al., 2019; Hampson et al., 2010; Hillary and Grafman, 2017; Hillary et al., 2015; Krishnadas et al., 2014).

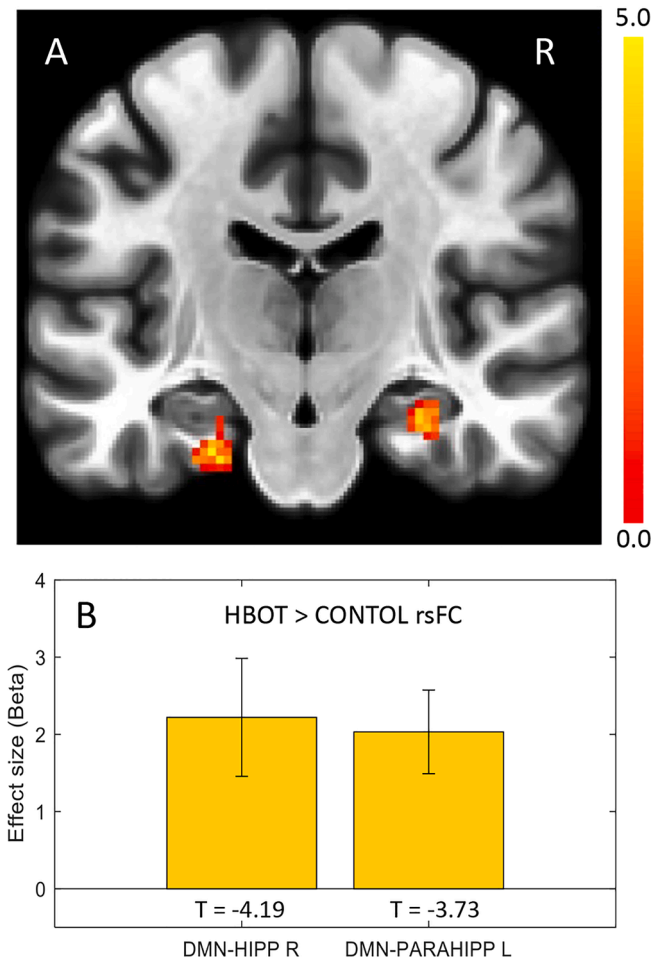

Fig. 3. Seed-to-voxel connectivity maps of longitudinal group differences in the hippocampus and parahippocampus. Group-by-time interaction ANOVA model in the DMN-MPFC seed region. A. Increased connectivity in the left parahippocampus (-24–18 −28, k = 68) and right hippocampus (28–18 −20, k = 75). B. Bar graphs of Fisher's Z effect size connectivity values for each cluster. $p < 0.05$, FWE corrected, k, cluster size, R, right.

Our results show that the strong trend of reduced connectivity, and reorganization of the triple-network rsFC was correlated with cognitive recovery.

Alterations in the olfactory brain network are associated with COVID-19 related hyposmia (Chung et al., 2021; Douaud et al., 2021; Esposito et al., 2022; Yildirim et al., 2022; Zhang et al., 2022). Although the pathogenesis of the post-COVID-19 condition is not yet determined, it was suggested that possible mechanisms include direct brain invasion of the virus, dysregulated immunologic responses, thrombotic disease, mitochondrial dysfunction and vascular injury with secondary tissue hypoxia (Silva Andrade et al., 2021; Yong and Liu, 2021). The olfactory brain structures, given their unique anatomical features, project to the orbitofrontal cortex, amygdala, hypothalamus, insula, entorhinal cortex, and hippocampus (Patel and Pinto, 2014). The olfactory region was suggested to serve as an entry zone to direct viral infection that impacts the hippocampus as secondary to the olfactory area (Najt et al., 2021). It has been shown that stress may reduce hippocampal volume and its connectivity with the ventromedial prefrontal cortex (Admon et al., 2013). Therefore, as anxiety is one of the major symptoms of post-COVID-19 condition (Shanbehzadeh et al., 2021), increased connectivity of the bilateral hippocampal rsFC with the medial prefrontal cortex (DMN-MPFC, BA10), induced by HBOT, may be linked to reformation of normal connectivity patterns and clinical relief from anxiety symptoms.

Post-COVID-19 condition is associated with long term psychiatric symptoms including depression, anxiety, and somatization (Stefano, 2021; Vanderlind et al., 2021). As shown in our previous publication, HBOT improved both depression and somatization symptoms in post-COVID-19 condition patients (Zilberman-Itskovich et al., 2022). An association between COVID-19 related psychiatric symptoms and alternations in rsFC has been demonstrated in several studies (Chen et al., 2021; Fu et al., 2021; Liu et al., 2021; Sheynin et al., 2020). In the current study, we observed increased connectivity between the amygdala and left angular gyrus and the primary sensory-motor area, which are associated with the execution of cognitive emotion regulation initiated by frontal areas (Kohn et al., 2014; Kropf et al., 2018). These changes have been correlated with improved psychiatric scores. Similar results were demonstrated in studies of depression and mental health problem suggesting that attenuated amygdala activity induce cortico-limbic rsFC alternations that may improve emotional regulation (Bershad et al., 2020; Pannekoek et al., 2014; Schreiner et al., 2017). Taken together, alternations in cognitive emotion regulation networks induced by HBOT may explain the clinical improvement in somatization and depression measures.

According to the MRI tractography, the structural connectivity from the left amygdala to other brain regions was significantly increased in the HBOT group compared to control, in means of FA, and subregion efficacy. The amygdala plays a crucial role in emotion processing and cognitive disorders by serving an important hub of anatomical connections to other limbic and cortical regions (Barbas, 2000). It has been shown that a reduction of anisotropy in the amygdala circuit indicates lower WM microstructure integrity which was associated in psychiatric disorders, depression, and aging (Burzynska et al., 2010; Ho et al., 2019; Podwalski et al., 2021). Furthermore, Qin et al. demonstrated widespread decreases in volume, length, and the mean FA value in association, commissural, projection, and limbic fiber bundles in mild and severe patients recovered from COVID-19 without neurological manifestations at the 3-month follow-up study (Qin et al., 2021). Persistent WM changes were also found in post COVID-19 patients at the 1-year

Table 4
Effects of cognitive and psychiatric scores on rs-FC between amygdala and insula seeds and post-hoc target clusters.

Seed	Cluster size	x	y	z	Anatomical Labels	Network	BA	T	P_{FWE}-value	P_{UNC}-value	Effect
BSI-18											
Amygdala (L)	85	−50	−60	48	Angular gyrus (L)	FPN	39	−4.33	0.012	0.0004	↑ rsFC ↓ BSI
Amygdala (R)	235	17	−31	80	Prim sensory (R)	SMN	1	−6.03	0.003	0.0001	↑ rsFC ↓ BSI
		3	−27	71	Prim motor (R)	SMN	4	−3.86	0.041	0.0003	↑ rsFC ↓ BSI
Insular cortex (L)	343	−44	−64	50	Angular gyrus (L)	FPN	39	4.68	< 0.0001	0.0000	↓ rsFC ↓ BSI
EF											
Amygdala (R)	84	58	−40	36	Sumpermarginal gyrus (R)	SN	40	4.30	0.039	0.0022	↑ rsFC ↑ EF
Amygdala (R)	42	−56	−38	30	Sumpermarginal gyrus (L)	SN	40	3.29	0.050	0.0010	↑ rsFC ↑ EF
IPS											
Amygdala (R)	136	−54	28	8	Broca (L)	LANG	45	4.53	0.008	0.0000	↑ rsFC ↑ IPS
Amygdala (L)	84	−54	26	8	Broca (L)	LANG	45	4.33	0.047	0.0023	↑ rsFC ↑ IPS

Fronto-parietal (FPN), salience network (SN), sensorimotor (SMN), language (LANG), EF, executive function, IPS, information processing speed, UNC, uncorrected, FWE, family-wise error. coordinates: x, sagittal, y, coronal, z, axial, refers to Montreal Neurological Institute (MNI), BA, Brodmann area, R, right, L, left.

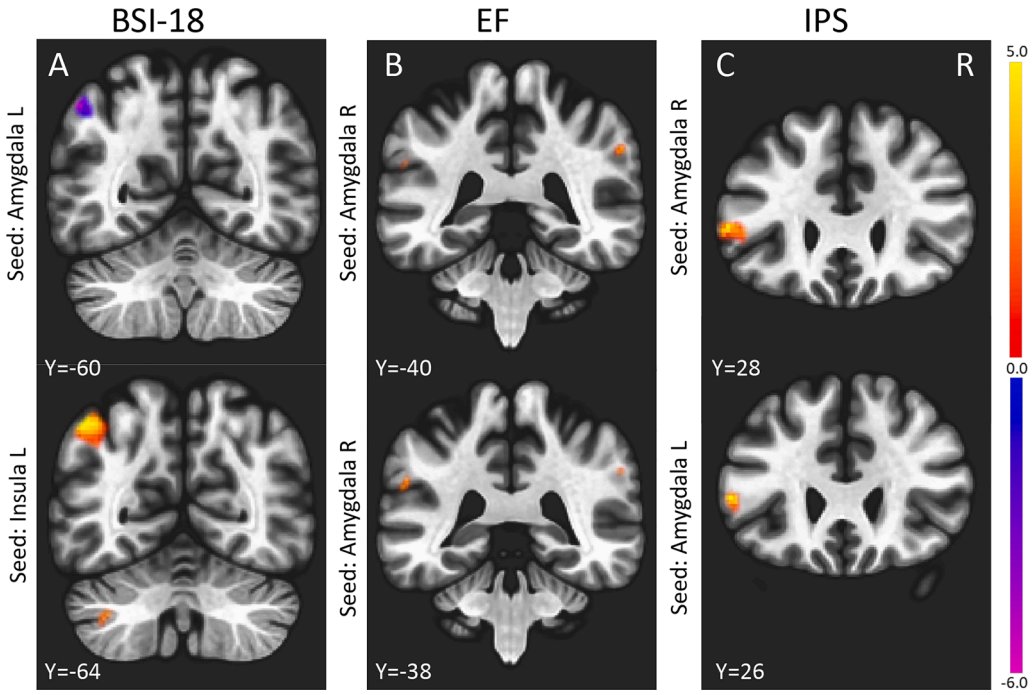

Fig. 4. Correlations of longitudinal differences in rsFC and cognitive and psychiatric scores in all patients (n = 56). (A) BSI-18 score negative correlation with amygdala-angular gyrus rsFC; positive correlation with insula-angular gyrus rsFC. (B) EF score: positive correlation with amygdala-sumpermarginal gyrus rsFC; (C) IPS score: positive correlation with amygdala-Broca area rsFC; P < 0.05, FWE corrected, R, right (see also Table 4).

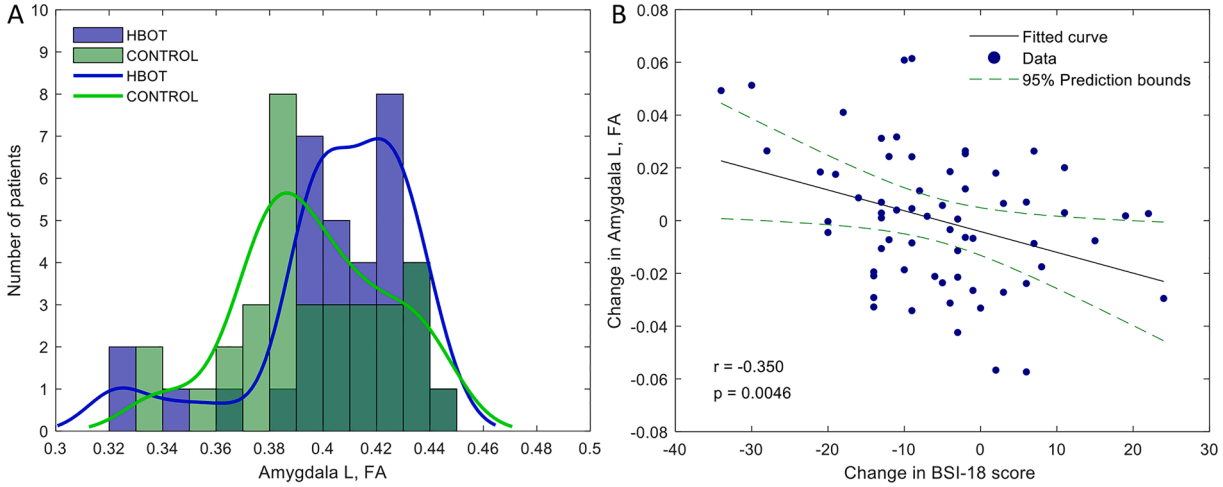

Fig. 5. Group differences in post treatment FA structural connectivity of the left amygdala. A. HBOT group (blue) patients showed increased FA of the amygdala tracts. Histogram and a distribution fit. B. Scatterplot of the change in FA, and the change in the BSI-18 score. The r is the Pearson's correlation coefficient. The 95% prediction interval is presented as a green line; FA, fractional anisotropy. (For interpretation of the references to color in this figure legend, the reader is referred to the web version of this article.)

follow-up study (Huang et al., 2022). Hence, increases in FA and structural efficacy may indicate response to treatment through improvement in WM fibers integrity.

The primary limitation of this study is the heterogeneity of clinical characteristics observed in this cohort, along with the relatively small sample size (symptom severity, time from infection, vaccination status, and post-COVID-19 symptoms) which may limit the ability to generalize from our findings. However, the longitudinal sham protocol provides a reliable control condition. Although rsFC has been widely used to explore longitudinal and group modifications, head motion is still a confounding factor due to the relatively long examination (Power et al., 2015) which resulted in a large dropout group and a potential for underpowered outcome estimation. Lastly, results were collected 1–3 weeks after the last HBOT session, and long-term results remain to be collected.

In conclusion, this study indicates that HBOT improves disruptions in WM tracts and alter functional connectivity organization of neural pathways attributed to cognitive and emotional recovery in post-COVID-19 patients. This study highlights the potential of structural and functional connectivity analysis as a promising treatment eligibility and response monitoring tool.

Funding

The study was funded by the research fund of Shamir Medical center, Israel.

CRediT authorship contribution statement

Merav Catalogna: Conceptualization, Methodology, Writing – original draft, Formal analysis. **Efrat Sasson:** Conceptualization, Methodology, Formal analysis, Writing – review & editing. **Amir Hadanny:** Conceptualization, Writing – review & editing. **Yoav Parag:** Investigation, Writing – review & editing. **Shani Zilberman-Itskovich:** Conceptualization, Investigation. **Shai Efrati:** Conceptualization, Writing – review & editing, Supervision, Funding acquisition.

Declaration of Competing Interest

The authors declare the following financial interests/personal relationships which may be considered as potential competing interests: AH and ES work for AVIV Scientific LTD. SE is a shareholder at AVIV Scientific LTD.

Data availability

Data will be made available on request.

Acknowledgments

We would like to acknowledge Fanny Atar, and the Livnat MRI unit, SMC, for their dedicated work. We would also like to thank Dr. Mechael Kanovsky for his editing of this manuscript.

Appendix A. Supplementary data

Supplementary data to this article can be found online at https://doi.org/10.1016/j.nicl.2022.103218.

References

Admon, R., Leykin, D., Lubin, G., Engert, V., Andrews, J., Pruessner, J., Hendler, T.J.H.b.m., 2013. Stress-induced reduction in hippocampal volume and connectivity with the ventromedial prefrontal cortex are related to maladaptive responses to stressful military service. 34, 2808-2816.

Alexander, A.L., Hasan, K., Kindlmann, G., Parker, D.L., Tsuruda, J.S.J.M.R.i.M.A.O.J.o.t.I.S.f.M.R.i.M., 2000. A geometric analysis of diffusion tensor measurements of the human brain. 44, 283-291.

Amir, H., Malka, D.-K., Gil, S., Rahav, B.-G., Merav, C., Kobi, D., Yafit, H., Ramzia, A.H., Efrat, S., Gregory, F., 2020. Cognitive enhancement of healthy older adults using hyperbaric oxygen: a randomized controlled trial. Aging 12.

Barbas, H.J.B.r.b., 2000. Connections underlying the synthesis of cognition, memory, and emotion in primate prefrontal cortices. 52, 319-330.

Behzadi, Y., Restom, K., Liau, J., Liu, T.T., 2007. A component based noise correction method (CompCor) for BOLD and perfusion based fMRI. Neuroimage 37, 90–101.

Benedetti, F., Palladini, M., Paolini, M., Melloni, E., Vai, B., De Lorenzo, R., Furlan, R., Rovere-Querini, P., Falini, A., Mazza, M.G.J.B., behavior, immunity-health, 2021. Brain correlates of depression, post-traumatic distress, and inflammatory biomarkers in COVID-19 survivors: A multimodal magnetic resonance imaging study. 18, 100387.

Benjamini, Y., Hochberg, Y., 1995. Controlling the false discovery rate: a practical and powerful approach to multiple testing. J. Roy. Stat. Soc.: Ser. B (Methodol.) 57, 289–300.

Bershad, A.K., Preller, K.H., Lee, R., Keedy, S., Wren-Jarvis, J., Bremmer, M.P., de Wit, H.J.B.P.C.N., Neuroimaging, 2020. Preliminary report on the effects of a low dose of LSD on resting-state amygdala functional connectivity. 5, 461-467.

Brkic, P., Stojiljkovic, M., Jovanovic, T., Dacic, S., Lavrnja, I., Savic, D., Parabucki, A., Bjelobaba, I., Rakic, L., Pekovic, S., 2012. Hyperbaric oxygenation improves locomotor ability by enhancing neuroplastic responses after cortical ablation in rats. Brain Inj. 26, 1273–1284.

Bullmore, E.T., Suckling, J., Overmeyer, S., Rabe-Hesketh, S., Taylor, E., Brammer, M.J., 1999. Global, voxel, and cluster tests, by theory and permutation, for a difference between two groups of structural MR images of the brain. IEEE Trans. Med. Imaging 18, 32–42.

Burzynska, A.Z., Preuschhof, C., Bäckman, L., Nyberg, L., Li, S.-C., Lindenberger, U., Heekeren, H.R.J.N., 2010. Age-related differences in white matter microstructure: region-specific patterns of diffusivity. 49, 2104-2112.

Ceban, F., Ling, S., Lui, L.M., Lee, Y., Gill, H., Teopiz, K.M., Rodrigues, N.B., Subramaniapillai, M., Di Vincenzo, J.D., Cao, B.J.B., behavior,, immunity, 2022. Fatigue and cognitive impairment in Post-COVID-19 Syndrome: A systematic review and meta-analysis. 101, 93-135.

Chen, Z., Feng, P., Becker, B., Xu, T., Nassar, M.R., Sirois, F., Hommel, B., Zhang, C., He, Q., Qiu, J.J.N.o.s., 2021. Neural connectome prospectively encodes the risk of post-traumatic stress disorder (PTSD) symptom during the COVID-19 pandemic. 15, 100378.

Chung, T.W.-H., Zhang, H., Wong, F.K.-C., Sridhar, S., Chan, K.-H., Cheng, V.C.-C., Yuen, K.-Y., Hung, I.F.-N., Mak, H.K.-F.J.B.s., 2021. Neurosensory rehabilitation and olfactory network recovery in Covid-19-related olfactory dysfunction. 11, 686.

Desikan, R.S., Ségonne, F., Fischl, B., Quinn, B.T., Dickerson, B.C., Blacker, D., Buckner, R.L., Dale, A.M., Maguire, R.P., Hyman, B.T., 2006. An automated labeling system for subdividing the human cerebral cortex on MRI scans into gyral based regions of interest. Neuroimage 31, 968–980.

Doniger, G.M., 2007. Mindstreams Computerized Cognitive Tests: Test Descriptions. Available: http://www.mirror.upsite.co.il/uploaded/files/1383_e7d7d3d98c924f036d3123733419149d.pdf. Accessed 05 July 2013.

Doniger, G.M., 2012. Guide to MindStreams Normative Data. Available: http://www.mirror.upsite.co.il/uploaded/files/1383_b44d4786c91058be301cb09a94ba70f4.pdf. Accessed 05 July 2013.

Douaud, G., Lee, S., Alfaro-Almagro, F., Arthofer, C., Wang, C., Lange, F., Andersson, J.L., Griffanti, L., Duff, E., Jbabdi, S.J.M., 2021. Brain imaging before and after COVID-19 in UK Biobank.

Douaud, G., Lee, S., Alfaro-Almagro, F., Arthofer, C., Wang, C., McCarthy, P., Lange, F., Andersson, J.L., Griffanti, L., Duff, E.J.N., 2022. SARS-CoV-2 is associated with changes in brain structure in UK. Biobank. 604, 697–707.

Duan, K., Premi, E., Pilotto, A., Cristillo, V., Benussi, A., Libri, I., Giunta, M., Bockholt, H.J., Liu, J., Campora, R.J.N.o.s., 2021. Alterations of frontal-temporal gray matter volume associate with clinical measures of older adults with COVID-19. 14, 100326.

Efrati, S., Ben-Jacob, E., 2014. Reflections on the neurotherapeutic effects of hyperbaric oxygen. Expert Rev. Neurother. 14, 233–236.

Egbert, A.R., Cankurtaran, S., Karpiak, S.J.B., behavior,, immunity, 2020. Brain abnormalities in COVID-19 acute/subacute phase: a rapid systematic review. 89, 543-554.

Esposito, F., Cirillo, M., De Micco, R., Caiazzo, G., Siciliano, M., Russo, A.G., Monari, C., Coppola, N., Tedeschi, G., Tessitore, A.J.H.B.M., 2022. Olfactory loss and brain connectivity after COVID-19. 43, 1548-1560.

Eyler, L.T., Elman, J.A., Hatton, S.N., Gough, S., Mischel, A.K., Hagler, D.J., Franz, C.E., Docherty, A., Fennema-Notestine, C., Gillespie, N.J.J.o.A.s.D., 2019. Resting state abnormalities of the default mode network in mild cognitive impairment: a systematic review and meta-analysis. 70, 107-120.

Fazekas, F., Chawluk, J.B., Alavi, A., Hurtig, H.I., Zimmerman, R.A.J.A.J.o.N., 1987. MR signal abnormalities at 1.5 T in Alzheimer's dementia and normal aging. 8, 421-426.

Fischer, D., Snider, S.B., Barra, M.E., Sanders, W.R., Rapalino, O., Schaefer, P., Foulkes, A.S., Bodien, Y.G., Edlow, B.L.J.N., 2022. Disorders of Consciousness Associated With COVID-19: A Prospective Multimodal Study of Recovery and Brain Connectivity. 98, e315-e325.

Fritz, C., 2011. E Morris P, J Richler J. Effect Size Estimates: Current Use, Calculations, and Interpretation. J. Exp. Psychol. Gen. 8, 2–18.

Fu, Z., Tu, Y., Calhoun, V.D., Zhang, Y., Zhao, Q., Chen, J., Meng, Q., Lu, Z., Hu, L.J.N.o.s., 2021. Dynamic functional network connectivity associated with post-traumatic stress symptoms in COVID-19 survivors. 15, 100377.

Gottfried, I., Schottlender, N., Ashery, U., 2021. Hyperbaric Oxygen Treatment-From Mechanisms to Cognitive Improvement. Biomolecules 11.

Hadanny, A., Efrati, S., 2020. The Hyperoxic-Hypoxic Paradox. Biomolecules 10.

Hafiz, R., Gandhi, T.K., Mishra, S., Prasad, A., Mahajan, V., Natelson, B.H., Di, X., Biswal, B.B.J.b., 2022. Assessing functional connectivity differences and work-related fatigue in surviving COVID-negative patients.

Hagmann, P., Cammoun, L., Gigandet, X., Meuli, R., Honey, C.J., Wedeen, V.J., Sporns, O.J.P.b., 2008. Mapping the structural core of human cerebral cortex. 6, e159.

Hampson, M., Driesen, N., Roth, J.K., Gore, J.C., Constable, R.T.J.M.r.i., 2010. Functional connectivity between task-positive and task-negative brain areas and its relation to working memory performance. 28, 1051-1057.

Han, Q., Zheng, B., Daines, L., Sheikh, A.J.P., 2022. Long-Term sequelae of COVID-19: A systematic review and meta-analysis of one-year follow-up studies on post-COVID symptoms. 11, 269.

Herridge, M.S., Azoulay, É.J.T.L.R.M., 2022. The COVID-19 continuum of illness.

Hillary, F.G., Grafman, J.H.J.T.i.c.s., 2017. Injured brains and adaptive networks: the benefits and costs of hyperconnectivity. 21, 385-401.

Hillary, F.G., Roman, C.A., Venkatesan, U., Rajtmajer, S.M., Bajo, R., Castellanos, N.D.J.N., 2015. Hyperconnectivity is a fundamental response to neurological disruption. 29, 59.

Ho, N.F., Chong, P.L.H., Lee, D.R., Chew, Q.H., Chen, G., Sim, K.J.H.R.o.P., 2019. The amygdala in schizophrenia and bipolar disorder: a synthesis of structural MRI, diffusion tensor imaging, and resting-state functional connectivity findings. 27, 150-164.

Huang, S., Zhou, Z., Yang, D., Zhao, W., Zeng, M., Xie, X., Du, Y., Jiang, Y., Zhou, X., Yang, W.J.B., 2022. Persistent white matter changes in recovered COVID-19 patients at the 1-year follow-up. 145, 1830-1838.

Katal, S., Balakrishnan, S., Gholamrezanezhad, A.J.J.o.N., 2021. Neuroimaging and neurologic findings in COVID-19 and other coronavirus infections: a systematic review in 116 patients. 48, 43-50.

Kohn, N., Eickhoff, S.B., Scheller, M., Laird, A.R., Fox, P.T., Habel, U.J.N., 2014. Neural network of cognitive emotion regulation—an ALE meta-analysis and MACM analysis. 87, 345-355.

Krishnadas, R., Ryali, S., Chen, T., Uddin, L., Supekar, K., Palaniyappan, L., Menon, V.J.T.L., 2014. Resting state functional hyperconnectivity within a triple network model in paranoid schizophrenia. 383, S65.

EKropf, E., Syan, S.K., Minuzzi, L., Frey, B.N.J.B.J.o.P., 2018. From anatomy to function: the role of the somatosensory cortex in emotional regulation. 41, 261-26.

Leemans, A., Jeurissen, B., Sijbers, J., Jones, D.K., 2009. ExploreDTI: a graphical toolbox for processing, analyzing, and visualizing diffusion MR data. Proc Intl Soc Mag Reson Med, p. 3537.
Liu, P., Yang, W., Zhuang, K., Wei, D., Yu, R., Huang, X., Qiu, J.J.N.o.s., 2021. The functional connectome predicts feeling of stress on regular days and during the COVID-19 pandemic. 14, 100285.
Menon, V., D'Esposito, M.J.N., 2022. The role of PFC networks in cognitive control and executive function. 47, 90-103.
Menon, V.J.T.i.c.s., 2011. Large-scale brain networks and psychopathology: a unifying triple network model. 15, 483-506.
Michelen, M., Manoharan, L., Elkheir, N., Cheng, V., Dagens, A., Hastie, C., O'Hara, M., Suett, J., Dahmash, D., Bugaeva, P.J.B.G.H., 2021. Characterising long COVID: a living systematic review. 6, e005427.
Miller, E.K., Cohen, J.D.J.A.r.o.n., 2001. An integrative theory of prefrontal cortex function. 24, 167-202.
Najt, P., Richards, H.L., Fortune, D.G.J.B., behavior,, immunity-health, 2021. Brain imaging in patients with COVID-19: A systematic review. 16, 100290.
Niroumand Sarvandani, M., Sheikhi Koohsar, J., Rafaiee, R., Saeedi, M., Seyedhosseini Tamijani, S.M., Ghazvini, H., Sheybani, H.J.B., Neuroscience, C., COVID-19 and the Brain: A Psychological and Resting-state fMRI Study of the Whole-brain Functional Connectivity. 0-0.
Pannekoek, J.N., Van Der Werff, S., Meens, P.H., van den Bulk, B.G., Jolles, D.D., Veer, I. M., van Lang, N.D., Rombouts, S.A., van der Wee, N.J., Vermeiren, R.R.J.J.o.C.P., Psychiatry, 2014. Aberrant resting-state functional connectivity in limbic and salience networks in treatment-naive clinically depressed adolescents. 55, 1317-1327.
Patel, R.M., Pinto, J.M.J.C.a., 2014. Olfaction: anatomy, physiology, and disease. 27, 54-60.
Podwalski, P., Szczygieł, K., Tyburski, E., Sagan, L., Misiak, B., Samochowiec, J.J.P.R., 2021. Magnetic resonance diffusion tensor imaging in psychiatry: A narrative review of its potential role in diagnosis. 73, 43-56.
Power, J.D., Schlaggar, B.L., Petersen, S.E., 2015. Recent progress and outstanding issues in motion correction in resting state fMRI. Neuroimage 105, 536–551.
Qin, Y., Wu, J., Chen, T., Li, J., Zhang, G., Wu, D., Zhou, Y., Zheng, N., Cai, A., Ning, Q., 2021. Long-term microstructure and cerebral blood flow changes in patients recovered from COVID-19 without neurological manifestations. J. Clin. Investig. 131.
Rockswold, S.B., Rockswold, G.L., Zaun, D.A., Zhang, X., Cerra, C.E., Bergman, T.A., Liu, J., 2010. A prospective, randomized clinical trial to compare the effect of hyperbaric to normobaric hyperoxia on cerebral metabolism, intracranial pressure, and oxygen toxicity in severe traumatic brain injury. J. Neurosurg. 112, 1080–1094.
Schreiner, M.W., Klimes-Dougan, B., Mueller, B.A., Eberly, L.E., Reigstad, K.M., Carstedt, P.A., Thomas, K.M., Hunt, R.H., Lim, K.O., Cullen, K.R.J.J.o.a.d., 2017. Multi-modal neuroimaging of adolescents with non-suicidal self-injury: Amygdala functional connectivity. 221, 47-55.
Shanbehzadeh, S., Tavahomi, M., Zanjari, N., Ebrahimi-Takamjani, I., Amiri-Arimi, S.J.J. o.p.r., 2021. Physical and mental health complications post-COVID-19: Scoping review. 147, 110525.
Sheynin, J., Duval, E.R., Lokshina, Y., Scott, J.C., Angstadt, M., Kessler, D., Zhang, L., Gur, R.E., Gur, R.C., Liberzon, I.J.N.C., 2020. Altered resting-state functional connectivity in adolescents is associated with PTSD symptoms and trauma exposure. 26, 102215.
Silva Andrade, B., Siqueira, S., de Assis Soares, W.R., de Souza Rangel, F., Santos, N.O., Dos Santos Freitas, A., Ribeiro da Silveira, P., Tiwari, S., Alzahrani, K.J., Goes-Neto, A., Azevedo, V., Ghosh, P., Barh, D., 2021. Long-COVID and Post-COVID Health Complications: An Up-to-Date Review on Clinical Conditions and Their Possible Molecular Mechanisms. Viruses 13.
Silva, L.S., Joao, R.B., Nogueira, M.H., Aventurato, I.K., de Campos, B.M., de Brito, M.R., Alvim, M.K.M., Ludwig, G.V.N., Rocha, C., Souza, T.K.A.S., 2021. Functional and microstructural brain abnormalities, fatigue, and cognitive dysfunction after mild COVID-19. medRxiv.
Soravia, L.M., Denier, N., Moggi, F., Grieder, M., Federspiel, A., Tschuemperlin, R.M., Batschelet, H.M., Vollstädt-Klein, S., Wiest, R., Stein, M.J.A.b., 2022. Reduced structural connectivity of the amygdala is associated with childhood trauma in adult patients with alcohol use disorder. 27, e13164.
Stefano, G.B., 2021. Historical Insight into Infections and Disorders Associated with Neurological and Psychiatric Sequelae Similar to Long COVID. Med. Sci. Monit. 27, e931447.
Tu, Y., Zhang, Y., Li, Y., Zhao, Q., Bi, Y., Lu, X., Kong, Y., Wang, L., Lu, Z., Hu, L.J.M.P., 2021. Post-traumatic stress symptoms in COVID-19 survivors: a self-report and brain imaging follow-up study. 26, 7475-7480.
Tzourio-Mazoyer, N., Landeau, B., Papathanassiou, D., Crivello, F., Etard, O., Delcroix, N., Mazoyer, B., Joliot, M.J.N., 2002. Automated anatomical labeling of activations in SPM using a macroscopic anatomical parcellation of the MNI MRI single-subject brain. 15, 273-289.
Vanderlind, W.M., Rabinovitz, B.B., Miao, I.Y., Oberlin, L.E., Bueno-Castellano, C., Fridman, C., Jaywant, A., Kanellopoulos, D., 2021. A systematic review of neuropsychological and psychiatric sequalae of COVID-19: implications for treatment. Curr Opin Psychiatry 34, 420–433.
Whitfield-Gabrieli, S., Nieto-Castanon, A., 2012. Conn: a functional connectivity toolbox for correlated and anticorrelated brain networks. Brain Connect. 2, 125–141.
WHO. Coronavirus disease 2019 (COVID-19) situation report (https://covid19.who.int/).
Yildirim, D., Kandemirli, S.G., Sanli, D.E.T., Akinci, O., Altundag, A.J.A.R., 2022. A comparative olfactory MRI, DTI and fMRI study of COVID-19 related anosmia and post viral olfactory dysfunction. 29, 31-41.
Yong, S.J., Liu, S., 2021. Proposed subtypes of post-COVID-19 syndrome (or long-COVID) and their respective potential therapies. In: Reviews in Medical Virology, p. e2315.
Zhang, H., Chung, T.W.-H., Wong, F.K.-C., Hung, I.F.-N., Mak, H.K.-F.J.B.s., 2022. Changes in the Intranetwork and Internetwork Connectivity of the Default Mode Network and Olfactory Network in Patients with COVID-19 and Olfactory Dysfunction. 12, 511.
Zilberman-Itskovich, S., Catalogna, M., Sasson, E., Elman-Shina, K., Hadanny, A., Lang, E., Finci, S., Polak, N., Fishlev, G., Korin, C., Shorer, R., Parag, Y., Sova, M., Efrati, S., 2022. Hyperbaric oxygen therapy improves neurocognitive functions and symptoms of post-COVID condition: randomized controlled trial. Sci. Rep. 12, 11252.